DOI: https://doi.org/10.15407/rpra30.04.285
UDC 621.375.4
PACS number: 07.57.-c

I.K. Kuzmychov [1], O.S. Lukash[1], O.B. Senkevych[1], O.A. Voitovych[1], T.M. Narytnyk [2], G.I. Churyumov [3]

[1] O.Ya. Usikov Institute for Radiophysics and Electronics of the NAS of Ukraine
12, Acad. Proskury St., Kharkiv, 61085, Ukraine
[2] Educational and Research Institute of Telecommunication Systems
of the National Technical University of Ukraine
"Igor Sikorsky Kyiv Polytechnic Institute"
37, Beresteiskyi Ave., Kyiv, 03056, Ukraine
[3] Harbin Institute of Technology
92, Xida St., Nangang, Harbin, Heilongjiang, 150001, China
E-mail: kuzmichev.igr@gmail.com

AXIALLY SYMMETRIC MODES IN AN OPEN RESONATOR

Subject and Purpose. *The behavior of axially symmetric oscillations in a hemispherical open resonator (OR) integrated into a waveguide transmission line and operating in pass-through mode is studied. The apertures of the OR mirrors are 60 mm. The radius of curvature of the spherical mirror is 85 mm. Two 3.6×0.17 mm slot coupling elements are positioned symmetrically about the OR axis and 13.2 mm away from it. The axially symmetric oscillations excited in a hemispherical OR by slotted coupling elements are analyzed with the view of characterizing dielectric materials using resonant methods in the EHF range.*

Methods and Methodology. *Basic quasi-optical techniques are adopted. Namely, the electric-field structures of oscillation types are measured by the perturbation method. The resonant transmission coefficients of open oscillatory systems and the physical phenomena occurring within them are experimentally studied using standard microwave measurement techniques.*

Results. *In the experimental study conducted at 70.622 GHz, OR oscillations with large transverse indices were identified from amplitude distributions. The perturbation method was used with a 1 mm diameter probe. It has been shown that in non-axial OR excitation, axially symmetric oscillations are generated among others. Experimentally, a distinctive feature of those axially symmetric oscillations has been established, which is an area with zero electric-field intensity at the center of the cavity. For the investigated* $TEM^*_{0,1,12}$ *oscillation, this area is 6 mm in diameter.*

Conclusions. *It has been demonstrated that an open resonator with axially symmetric oscillations is effective for measuring the electrophysical parameters of materials, including liquids. It has been established that the placement of a disk-shaped sample or a liquid-filled cuvette at the center of the flat mirror of a hemispherical OR not only does not disrupt the working oscillation but additionally contributes to the angular mode selection of the OR oscillation spectrum. The hemispherical OR, as considered, can also be used for dynamic quality control of various liquids. In this case, the holder, like a quartz glass tube, is positioned along the OR axis.*

Keywords: *millimeter-wave range, open resonator, modes, coupling element, transmission coefficient, probe.*

Introduction

The measurement of the electrophysical properties of liquid dielectrics is an important problem in medicine, agriculture, and the oil industry. It poses significant challenges for determining moisture content in various solutions, oils, and petroleum-based liquids, as well as for their quality control [1—4]. Currently,

Citation: Kuzmychov, I.K., Lukash, O.S., Senkevych, O.B., Voitovych, O.A., Narytnyk, T.M., Churyumov, G.I., 2025. Axially symmetric modes in an open resonator. *Radio Phys. Radio Astron.*, **30**(4), pp. 285—295. https://doi.org/10.15407/rpra30.04.285

the free-space method [5, 6], the waveguide method [7—9], and the resonant method [10—13] are well-established techniques commonly used to characterize the electrophysical properties of both liquid and solid dielectrics in the Super-High Frequency (SHF) range. The resonant method using cavity resonators is often preferred due to its higher sensitivity. Typically, measurements are conducted at X band (8 to 12 GHz) [14, 15], which gains a balance between performance and practicality. Higher-frequency bands, such as Ka and especially V and W, can enhance measurement sensitivity. However, higher frequencies require smaller cavity dimensions and increase ohmic losses in the cavity walls, which results in a lower loaded *Q*-factor and degraded measurement accuracy. The use of lower-frequency bands L and S builds up the mass and overall size of the measurement setup.

Yet, despite the above considerations, the Extremely High Frequency (EHF) range is just right to measure the electrophysical parameters of liquid dielectrics [16, 17] because at EHF, the dielectric permittivity and loss tangent of water decrease [18]. Water is a major component of many biological fluids and may be present in oils and petroleum products. Yet, to apply the resonant method for measuring the electrophysical parameters of not only dielectric liquids but also solids, the resonant systems — open resonators (OR) — should be adapted for those high frequencies [19—27]. The most widespread are hemispherical resonators [20, 21, 23, 28, 29]. This is primarily because a plane-parallel sample [21, 30] or a liquid-filled cuvette [43] is accommodated on the OR flat mirror, near which the fundamental TEM_{00q} mode has its phase front flat. In measurements, care is taken that the transverse dimensions of the solid sample or the liquid-carrying cuvette exceed the diameter of the TEM_{00q} mode field spot on the mirror.

In [31], a hemispherical OR attached to a section of oversized circular waveguide is used for the characterization of solid dielectrics. Disk-shaped samples are accommodated at the bottom of the circular waveguide section, while cylindrical samples are positioned along the OR axis. The waveguide propagates the TE_{01} wave. To efficiently excite the TEM_{10q} mode in the OR, the coupling element on the spherical mirror was shifted away from the OR axis by 5.5 mm. A similar composite OR described in [32] differs from the previous OR structure [31] by supporting the higher-order axially asymmetric TEM_{30q} mode. To efficiently excite the TEM_{30q} mode, the coupling element on the curvilinear mirror is shifted 11.5 mm from the OR axis. It turns out that, along with the well-known modes [33], the resonator of that kind supports the axially symmetric modes $TEM^{\star}_{01q}$ and $TEM^{\star}_{11q}$ [34]; the asterisk here stands to denote that the oscillation is a quasi-mode. A distinctive feature of these modes is a zero-valued electric-field intensity within an extended area at the center of each mirror. Introduce a disk-shaped sample, or a cuvette, or a quartz glass tube filled with some liquid into that region, and use the OR method for the research into the electrophysical properties of various substances, including high-loss materials. The resonator design enables measurements in both static and dynamic modes.

The article discusses axially symmetric modes excited by a slot coupling element placed some distance from the curvilinear reflector axis in a hemispherical open resonator.

1. Experimental setup

A block diagram of the experimental setup for studying oscillation modes is shown in Fig. 1. An external view of the setup is in Fig. 2. According to Fig. 1, the hemispherical OR adopted for electrophysical measurements consists of spherical *1* and flat *2* mirrors. The apertures of both mirrors are $2a = 60$ mm. The curvature radius of the spherical mirror is $R = 85$ mm. The normalized mirror space L/R is approximately 0.6. The setup design follows the cathetometer principle.

Slot coupling element *3* in spherical mirror *1* feeds the signal into the OR. Coupling element *3* cites 13.2 mm away from the OR axis (the 0*z* axis, Fig. 3) and represents a rectangular waveguide taper between a standard cross-section of 3.6×1.8 mm and a smaller one of 3.6×0.17 mm. This coupling element enables efficient excitation of the high-order, axially asymmetric oscillation modes TEM_{10q} and TEM_{20q}. Under the TEM_{mnq} label, subscript m indicates the number of electric field nodes along the 0x axis, n stands for the number of nodes along the 0y axis, and q is the longitudinal index.

The signal source is a G4-142 generator, *6* in Fig. 1. It acts as a microwave oscillator, covering the 53.57 to 78.33 GHz range with a frequency setting error of 1% and a possible frequency instability within 15 MHz.

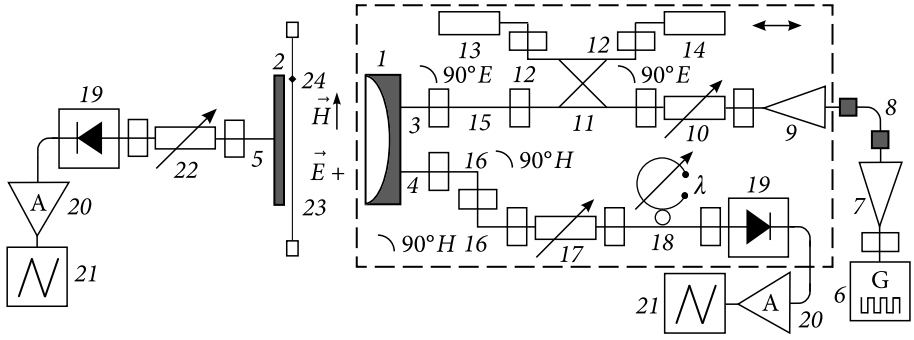

Fig. 1. Block diagram of the experimental setup

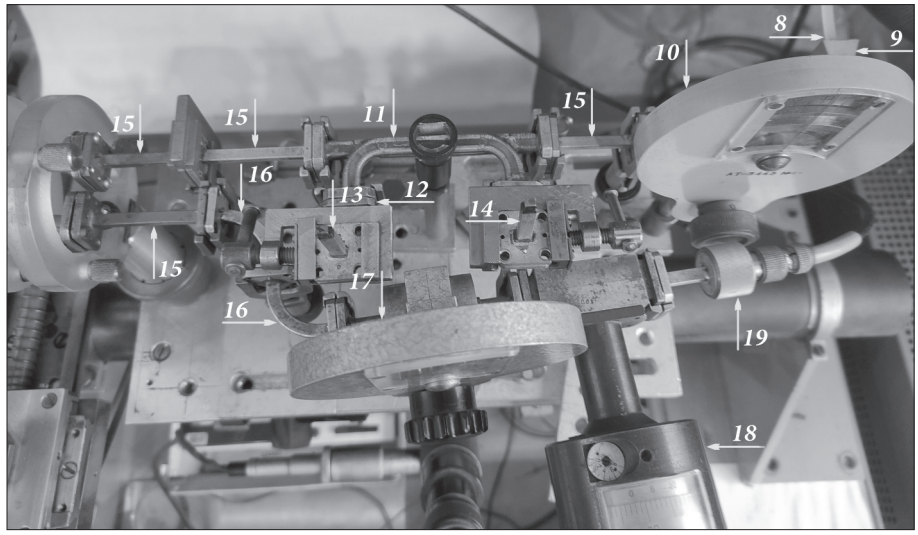

Fig. 2. The waveguide part of the experimental setup

The output power is at least 4×10^{-3} W, with the potential for smooth frequency tuning over a 100 MHz range. The output power is regulated within 0 to 30 dB. To expand the dynamic range during measurements, the generator output signal is amplitude-modulated by a 1 kHz frequency square wave. The working frequency is $f = 70.622$ GHz ($\lambda = 4.248$ mm).

From the cavity, the signal is extracted using 3.6×0.17 mm coupling element *4* (see Fig. 3), which is mirror-symmetrical about the OR axis to coupling element *3*. Coupling elements *3* and *4* are identical rectangular-waveguide tapers between standard 3.6×1.8 mm and smaller 3.6×0.17 mm cross-sections. Figures 1 and 3 show how the magnetic $(\vec{H})$ and electric $(\vec{E})$ field vectors of the TE_{10} wave are directed inside waveguide *3*.

The signal from generator 6 is directed to the waveguide path via a 3.6×2.0 mm polyethylene dielectric waveguide *8*. For more effective impedance matching between waveguide *8*, generator 6, and the waveguide path, two pyramidal horns *7* and *9* of 19.5 mm lengths and 14.5×11.5 mm apertures are inserted into the circuit. For additional decoupling between the cavity and generator *6*, a –8 dB fixed attenuator *10* is introduced. Directional coupler *11* in the waveguide path allows, if needed, monitoring of the cavity reflection coefficient during cavity tuning. The power coupled off the incident wave is directed through the *E*-plane waveguide bend *12* to a matched load *13*. The power coupled off the wave reflected from the cavity input is directed through the *E*-plane waveguide bend *12* to a matched load *14*.

The signal from generator *6* feeds into the cavity through waveguide sections *15* and coupling element *3* (see Fig. 2). The signal that has passed through the cavity is sent via coupling element *4* to the receiving path, which contains two *H*-plane waveguide bends *16*, polarization attenuator *17*, wavemeter *18*,

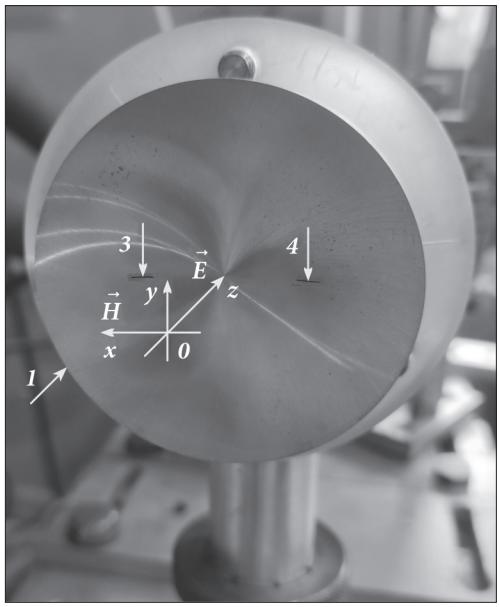

Fig. 3. The OR spherical mirror with the slot coupling elements

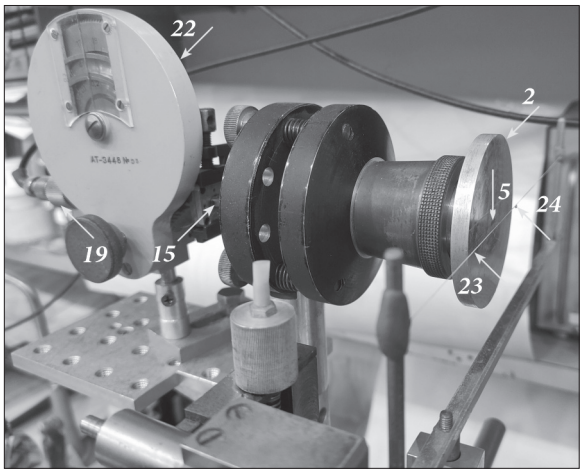

Fig. 4. The OR flat mirror with the slot coupling element

detector *19*, resonant amplifier *20*, and oscilloscope *21*. The wavemeter renders frequency monitoring of generator *6*.

The setup (see Figs. 1 and 4) includes an additional receiving path. The signal feeds into this path through coupling element *5* at the center of the OR flat mirror *2*. Similar to the other two coupling elements, *3* and *4*, coupling element *5* is also a taper from a standard 3.6×1.8 mm waveguide cross-section to a reduced cross-section of 3.6×0.16 mm. This waveguide path contains waveguide section *15*, measurement polarization attenuator *22*, detector *19*, resonant amplifier *20*, and oscilloscope *21* (see Fig. 4).

To identify oscillation types excited in the studied hemispherical OR, we use the perturbation (probe) method [35]. The electric field component distribution is measured using probe *24* (see Fig. 4) hanging on a 0.1 mm-thick nylon thread *23*.

The system is tuned to resonance by adjusting the spherical mirror (with the waveguide path attached) along the OR axis. This part of the experimental setup is highlighted with dashes in Fig. 1. The OR mirror space is measured with an accuracy of ±0.001 mm.

2. Measurement results

The excitation of the $TEM^{\star}_{01q}$ oscillation [34] in the cavity is considered. The signature of this oscillation is an area of zero electric field intensity at the center of the OR mirror. A sample of measurement results for the resonant transmission coefficient K_{transm} of the $TEM^{\star}_{01q}$ mode versus the normalized mirror space L/R is shown in Fig. 5. As the longitudinal oscillation index q increases by 1, the OR mirror space expands by approximately $\lambda/2$. At each q, the $TEM^{\star}_{01q}$ oscillation types were identified by the perturbation method.

According to Fig. 5, the OR transmission coefficient K_{transm} increases as the normalized mirror space L/R decreases because ohmic and diffraction losses of the OR decrease. At $L/R = 0.245$ (the $TEM^{\star}_{0,1,10}$ mode), the K_{transm} drops because the $TEM^{\star}_{0,1,10}$ interacts with another mode excited in the OR. The K_{transm} decrease for $L/R < 0.193$ is attributed to the wave mode coupling amid the crowding of the OR mode spectrum for small mirror spaces.

Let us estimate the loaded quality factor Q_L of the $TEM^{\star}_{0,1,12}$ mode. The fixed-frequency measurements admit the formula $Q_L = L_{res} / \Delta l$ [36], where L_{res} is the mirror space at which the $TEM^{\star}_{0,1,12}$ mode transmission is at its maximum, and $\Delta l = L_1 - L_2$, where L_1 and L_2 are the mirror spaces at which the transmission coefficient of the mode drops by half (–3 dB). Based on the experimental data, the loaded Q-factor of the $TEM^{\star}_{0,1,12}$ mode was found to be 2800.

The electric field structure of the $TEM^{\star}_{0,1,12}$ mode in the OR is worth considering in two mutually perpendicular planes: in the planes $x0z$ (the plane of the vector $\vec{H}$) and $y0z$ (the plane of the vector $\vec{E}$) (see Fig. 3). The z-axis coincides with the OR axis. The amplitude distribution of the electric field component of the $TEM^{\star}_{0,1,12}$ mode was measured at the

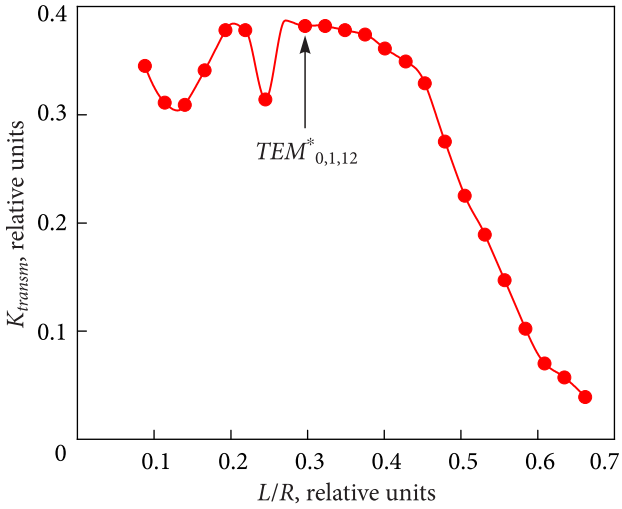

Fig. 5. The resonant transmission coefficient versus the OR mirror space for the axially symmetric TEM^{*}_{01q} oscillations

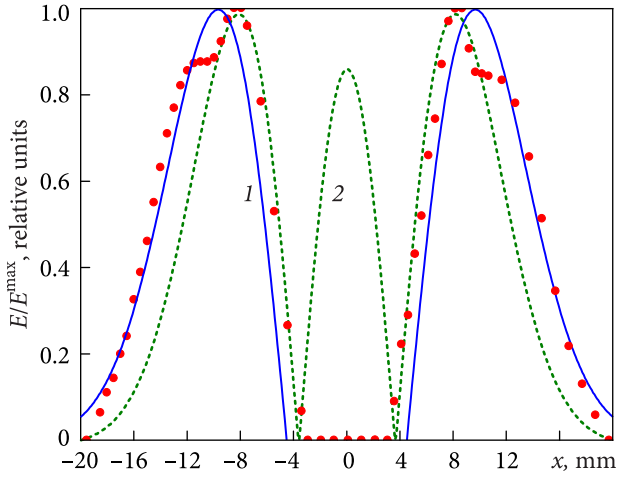

Fig. 6. The measured electric field structure of the $TEM^{*}_{0,1,12}$ mode (grey circles) and the calculated field distributions for the $TEM_{1,0,12}$ (curve *1*) and $TEM_{2,0,12}$ (curve *2*) modes in the hemispherical OR in the $x0z$ plane ($y=0$)

first antinode (counting from the flat mirror) of the standing-wave electric field component, i.e., at approximately $z=\lambda/4$. As already mentioned, the perturbation method performs these measurements. The diameter of the scattering (metallic) probe is determined by the OR loaded quality Q_L and the operating wavelength λ. Based on the results of work [37], the probe diameter was taken to be 1 mm.

The measured amplitude distribution of the electric-field component of the $TEM^{*}_{0,1,12}$ mode in the $x0z$ plane inside the OR is drawn with grey circles in Fig. 6.

In the $x0z$ plane, the investigated mode $TEM^{*}_{0,1,12}$ shows two field spots, forming a two-lobe field pattern. Of practical interest is to compare the electric-field amplitude distributions of the modes $TEM^{*}_{0,1,12}$ (measured) and the $TEM_{1,0,12}$ (simulated using Hermite-Gaussian functions) [33, 38, 39] because the electric field structures of the $TEM_{1,0,12}$ and $TEM^{*}_{0,1,12}$ modes are visually similar. The difference is that the $TEM^{*}_{0,1,12}$ mode has an area of zero electric field intensity at the OR mirror center.

The TEM_{10q} mode can be excited in the OR when the coupling element is shifted off the spherical mirror axis. The simulation of the electric-component amplitude distribution of the $TEM_{1,0,12}$ mode on the flat mirror requires the knowledge of the OR mirror space $L_{0,0,12}$ corresponding to the fundamental $TEM_{0,0,12}$ mode excitation. This step is essential because amplitude distributions of the electric field components of all the OR oscillation modes are expressed via the spot radius of the fundamental TEM_{00q} mode [39, 40]. When the coupling element is shifted to the periphery of the curvilinear mirror (see Fig. 3), the TEM_{00q} mode is not excited in the OR. This conclusion was experimentally verified using probe *24* (Fig. 4) and the waveguide channel connected to coupling element *5* located at the center of OR flat mirror *2* (Fig. 4).

The experimentally measured value of the OR mirror space at which the $TEM_{2,0,12}$ mode is excited is 26.68 mm. The field distribution of the $TEM_{2,0,12}$ oscillation, like that of the $TEM_{1,0,12}$, is described by Hermite-Gaussian functions. The next step is calculating the OR mirror space for the $TEM_{2,0,12}$ mode from the expression [38, 39]

$$f=\frac{c}{2L^{calcul}\times 10^{-3}}\times \left[q+(m+n+1)\frac{1}{\pi}\arccos\left(\sqrt{1-\frac{L^{calcul}}{R}}\right)\right]. \qquad (1)$$

Here, $f=70.622\times10^{9}$ Hz is the resonance frequency, $c=3\times10^{8}$ m/s is the speed of light, L^{calcul}, mm is the calculated OR mirror space, and $R=85$ mm is the curvature radius of the spherical mirror. Ibidem, $q=12$ is the longitudinal index of the $TEM_{2,0,12}$ mode, its transverse indices are $m=2$ (coordinate x, Fig. 3) and $n=0$ (coordinate y, Fig. 3). Substituting the numerical values into expression (1) yields $L^{calcul}_{2,0,12}=26.695$ mm. The discrepancy between the calculated and measured mirror spaces for the $TEM_{2,0,12}$ mode is 0.056%.

Similar evaluations are performed for the next mode, $TEM_{3,0,12}$. Its field structure is also described by Hermite-Gaussian functions. The measured value of its resonant mirror space is 27.096 mm. And the same as before for the $TEM_{2,0,12}$, but with $m = 3$, the resonant mirror space is calculated by formula (1). Substituting the numerical values into equation (1) yields the OR mirror space $L_{3,0,12}^{calcul} = 27.111$ mm. The discrepancy between the calculated and measured mirror spaces for the $TEM_{3,0,12}$ mode is 0.055%.

The calculated mirror space $L_{0,0,12}^{calcul}$ can be used to determine the radius of the $TEM_{0,0,12}$ mode spot on the flat mirror of the hemispherical OR. Given all the numerical values unchanged except the transverse index m, which for the fundamental mode is zero, we have the mirror space $L_{0,0,12}^{calcul} = 25.883$ mm from expression (1).

We calculate the spot radius of the $TEM_{0,0,12}$ mode on the OR flat mirror using the expression [38, 39]

$$w_0^{calcul} = \sqrt{\frac{\lambda}{\pi} R \sqrt{\frac{L_{0,0,12}^{calcul}}{R}\left(1 - \frac{L_{0,0,12}^{calcul}}{R}\right)}}, \qquad (2)$$

where $\lambda = 4.248$ mm as before. Substituting the numerical values into expression (2) yields the spot radius $w_0^{calcul} = 7.274$ mm for the $TEM_{0,0,12}$ mode.

The normalized theoretical distribution of the electric-field amplitude of the $TEM_{1,0,12}$ mode on the OR flat mirror in the $x0z$ plane ($y = 0$) is constructed by the formula [39]

$$\left| E / E^{\max} \right| = \left| \frac{\sqrt{2e}\, x}{w_0^{calcul}} \exp\left[-(x / w_0^{calcul})^2 \right] \right|. \qquad (3)$$

The calculation results produce curve *1* in Fig. 6. To compare the field structures of the $TEM^{\star}_{0,1,12}$ and $TEM_{1,0,12}$ modes, we superimpose their amplitude distributions. They match well, but there are two notable exceptions. The first is a roughly 5 mm-wide area with zero electric-field intensity, which the $TEM^{\star}_{0,1,12}$ mode shows at the center of the mirror — something not observed in the amplitude distribution of the electric field of the TEM_{1012} mode [33, 38, 39]. The other is a substantially different behavior that the electric-field amplitudes of the $TEM^{\star}_{0,1,12}$ and $TEM_{1,0,12}$ modes demonstrate within the domain $0.8 < \left| E/E^{\max} \right| < 1$ (Fig. 6).

To understand the behavior of the electric field intensity of the $TEM^{\star}_{0,1,12}$ mode, address the normalized amplitude distribution of the electric field intensity of the $TEM_{2,0,12}$ mode using the following expression [39]

$$\left| E/E^{\max} \right| = \frac{\left| \left(\left(\frac{2x}{w_0^{calcul}} \right)^2 - 1 \right) \exp\left[-(x/w_0^{calcul})^2 \right] \right|}{4\exp(-1.25)}. \qquad (4)$$

The calculations by formula (4) generate curve *2* in Fig. 6. As observed, the values $\left| E/E^{\max} \right| = 1$ at the positions $x = \pm(w_0^{calcul}\sqrt{5})/2 = \pm 8.133$ mm correspond to the side lobes of the $TEM_{2,0,12}$ mode field. The calculated x values are in close agreement with the experimentally measured x values at which the normalized electric field intensity of the $TEM^{\star}_{0,1,12}$ mode equals unity (see Fig. 6). Also, from Fig. 6 it follows that up to $x = \pm 9.614$ mm — which correspond to $\left| E/E^{\max} \right| = 1$ in the calculated distribution (curve *1*) of the electric field component of the $TEM_{1,0,12}$ mode — the electric field structure of the $TEM^{\star}_{0,1,12}$ oscillation closely coincides with the side lobes of the electric field component of the $TEM_{2,0,12}$ mode. Further to the periphery of the flat mirror, the electric field structure of the $TEM^{\star}_{0,1,12}$ mode fully aligns with that of the $TEM_{1,0,12}$ mode.

Thus, it can be concluded that the amplitude distribution of the electric field component of the investigated $TEM^{\star}_{0,1,12}$ mode represents a hybrid structure combining the features of the electric fields of the $TEM_{2,0,12}$ and $TEM_{1,0,12}$ modes. The main distinction of the investigated $TEM^{\star}_{0,1,12}$ mode from the conventional $TEM_{2,0,12}$ and $TEM_{1,0,12}$ modes lies in that the $TEM^{\star}_{0,1,12}$ mode exhibits a roughly 5 mm-wide area with zero electric field intensity at the center of the mirror (see Fig. 6).

For a better understanding of the electric field structure of the $TEM^{\star}_{0,1,12}$ mode inside the OR, the behavior of its electric field component should be analyzed in the $y0z$ plane (Fig. 3). The measurement results are shown in grey circles in Fig. 7.

The electric field intensity of the $TEM_{1,0,12}$ mode in the $y0z$ plane is zero due to the proper orientations of slot coupling elements *3* and *4* on the spherical mirror (Fig. 3). At the same time, this is not the case for the $TEM^{\star}_{0,1,12}$ mode. Figure 7 evidences that the amplitude distribution of the electric field of the $TEM^{\star}_{0,1,12}$ mode in the $y0z$ plane (the grey-circle

curve) resembles that of the $TEM_{1,0,12}$ mode in the $x0z$ plane (solid curve *1*). As before, we compare the field structures of the $TEM^{\star}_{0,1,12}$ and $TEM_{1,0,12}$ by superimposing their amplitude distributions.

The plots in Fig. 7 are qualitatively identical, with two exceptions. The first is that the investigated $TEM^{\star}_{0,1,12}$ mode in the $y0z$ plane (the same as in the plane $x0z$) shows a roughly 5 mm-wide area with zero electric-field intensity at the center of the mirror. The second is that the curve $\left|E/E^{\max}\right| = 1$ for the $TEM^{\star}_{0,1,12}$ mode reaches its maxima at $y = \pm 10.75$ mm, while the $TEM_{1,0,12}$ mode does so at ± 9.614 mm. Additionally, as in the previous $x0z$ case, the investigated $TEM^{\star}_{0,1,12}$ mode is slightly deformed in the high-intensity field domain $0.8 < \left|E/E^{\max}\right| < 1$. As before, this is likely due to the excitation of high-order modes in the OR with the coupling element shifted towards the mirror periphery. Thus, our research demonstrates that axially symmetric modes can still get excited in the OR when the coupling element is placed off the spherical mirror center, and this is true even though the resonator lacks axial symmetry (see Fig. 3).

If the coupling element is located at the center of the mirror, only modes with even transverse m indices (TEM_{00q}, TEM_{20q}, TEM_{40q}, ...) are excited in the resonator. The shifting of the coupling element toward the mirror periphery enhances the spectral crowding of this resonant system at the cost of the OR modes with odd m indices (TEM_{10q}, TEM_{30q}, TEM_{50q}, ...). Interestingly, in this case, the OR fundamental TEM_{00q} mode is not excited. And this was experimentally confirmed.

Let us consider a fragment of the measured OR mode spectrum illustrated in Fig. 8. The labelled oscillation types were identified using the perturbation method. In the indicated range of OR mirror spaces, both the modes $TEM_{1,0,12}$, $TEM_{3,0,12}$, $TEM_{5,0,11}$, and $TEM_{7,0,11}$ with zero electric-field intensity on the OR axis and the modes $TEM_{2,0,12}$, $TEM_{4,0,11}$, $TEM_{6,0,11}$, and $TEM_{8,0,11}$ with nonzero electric-field intensity on this OR axis are excited.

As observed (Fig. 8), within the indicated OR tuning range, the transmission coefficient is at a maximum not only for the $TEM^{\star}_{01q}$ mode but also for the $TEM_{3,0,12}$ and $TEM_{4,0,11}$. To understand why, address the $TEM_{3,0,12}$ mode. The normalized distribution of its electric field component on the OR spherical mirror is described by the formula [38, 39]

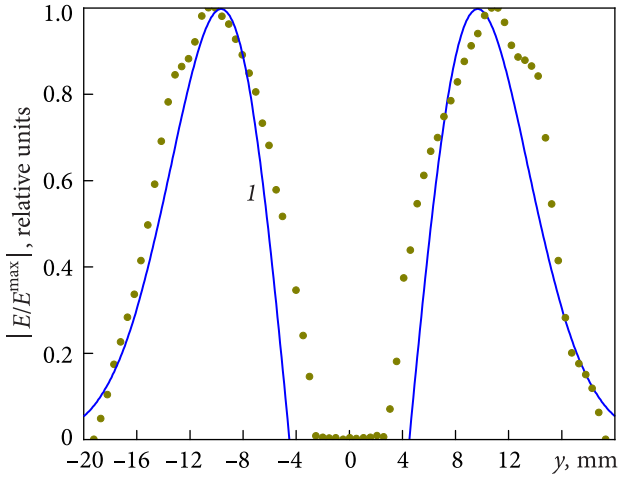

Fig. 7. The measured electric field distribution of the $TEM^{\star}_{0,1,12}$ mode in the plane $y0z$ ($x = 0$) (grey circles) and the calculated electric field distribution of the $TEM_{1,0,12}$ mode (curve *1*)

$$\left|E/E^{\max}\right| = \frac{\left|\left(8\left(\frac{\sqrt{2}x}{w_1^{calcul}}\right)^3 - 12\frac{\sqrt{2}x}{w_1^{calcul}}\right)\exp\left[-(x/w_1^{calcul})^2\right]\right|}{5.4226}. \quad (5)$$

Here, w_1^{calcul} is the spot radius of the fundamental $TEM_{0,0,12}$ mode on the OR spherical mirror,

$$w_1^{calcul} = \sqrt{\frac{\lambda}{\pi}R\sqrt{\frac{L_{0,0,12}^{calcul}/R}{1 - L_{0,0,12}^{calcul}/R}}}. \quad (6)$$

Substituting the numerical values of λ, R, and $L_{0,0,12}^{calcul}$ into equation (6) yields $w_1^{calcul} = 8.726$ mm. The spot radius (8.726 mm) of the fundamental $TEM_{0,0,12}$ mode on the spherical mirror is much smaller than the distance (13.2 mm) from the OR axis to the coupling element location. This explains why the $TEM_{0,0,12}$ mode is absent in the OR mode spectrum. From equation (5), we find that the positions $x_{1,2}$ of the electric field intensity maxima ($\left|E/E^{\max}\right| = 1$) of the $TEM_{3,0,12}$ mode on the curvilinear reflector are given by the expression $x_{1,2} = \pm(w_1^{calcul}/2)\sqrt{(9+\sqrt{57})/2}$. Substituting the obtained $w_1^{calcul} = 8.726$ mm yields $x_{1,2} = \pm 12.551$ mm. Compare it (12.551 mm) with the value (13.2 mm) of the above-mentioned offset of the coupling element on the spherical mirror from the OR axis. The difference is as small as 0.649 mm.

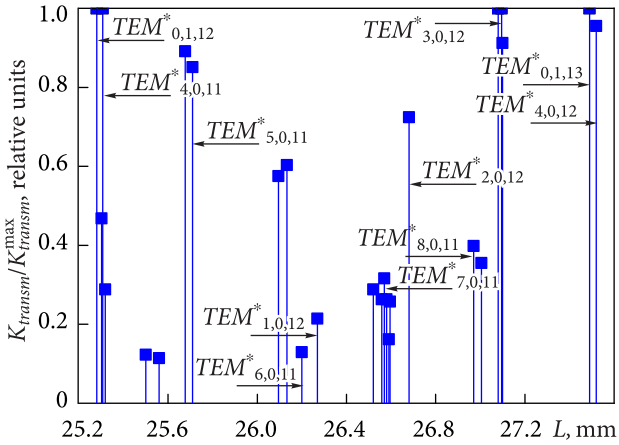

Fig. 8. A fragment of the mode spectrum of an empty hemispherical OR

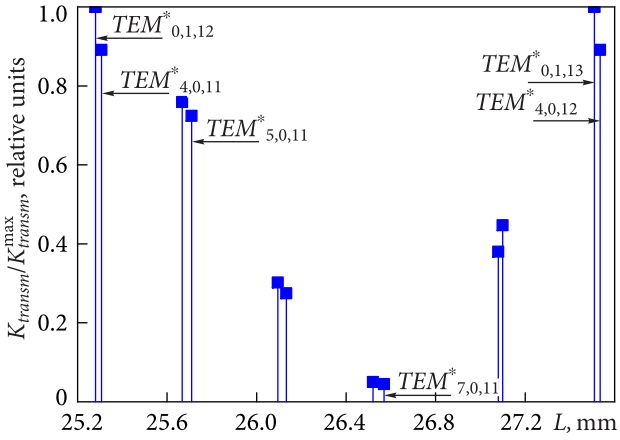

Fig. 9. A fragment of the mode spectrum of a hemispherical OR loaded with a brass disk placed at the center of the flat mirror

This explains the high transmission coefficient of the cavity in which the $TEM_{3,0,12}$ mode is excited.

The mode spectrum fragment in Fig. 8 suggests that the resonant system of this kind is unsuitable for measuring the electrophysical parameters of materials because of a large number of excited modes. This circumstance complicates the operating-mode identification when the sample is placed on the OR mirror. Carrying out these studies requires angular mode selection of the OR spectrum.

According to Figs. 6 and 7, the investigated mode $TEM^*_{0,1,12}$ displays an area with zero-valued electric-field intensity on the OR axis. Let a brass disk with a 5 mm diameter and a 1 mm height be placed at the center of the flat mirror. This disk does not affect the transmission coefficient on the modes $TEM^*_{0,1,12}$ and $TEM^*_{0,1,13}$. Yet, having a height of approximately $\lambda/4$, it creates a strong phase inhomogeneity in the OR. Also, let us line the edge of the flat mirror with absorbing graphite strips, arranged into a rectangular frame. Each strip is 4 mm wide, 10 mm long, and the edge is 5 mm away from the mirror edge. In this shape, the absorber does not affect the transmission coefficient of the investigated $TEM^*_{0,1,12}$ mode, which covers an area of about 40 mm in diameter on the flat mirror (see Fig. 6). A fragment of the OR spectrum when the above-mentioned additional components are inserted in the OR interior is shown in Fig. 9.

Compared to the empty OR spectrum in Fig. 8, the oscillation spectrum of the loaded OR in Fig. 9 is much sparser, with the transmission coefficient K_{transm} of the analyzed $TEM^*_{0,1,12}$ mode nearly unchanged. In the loaded OR, several OR modes ($TEM_{1,0,12}$, $TEM_{2,0,12}$, $TEM_{3,0,12}$, $TEM_{6,0,11}$, and $TEM_{8,0,11}$) are not excited at all. The empty-OR oscillations (e.g., $TEM_{5,0,11}$, $TEM_{7,0,11}$) have significantly reduced amplitudes. Thus, samples in the form of a disk or a liquid-carrying cuvette positioned at the center of the flat mirror contribute to the angular mode selection of the OR spectrum.

For measuring the electrophysical parameters of liquid dielectrics using a quartz glass tube placed along the OR axis, modifications to the OR design are required. Specifically, the area with zero electric-field intensity along the OR axis should be minimized. To this end, the radius of curvature of the spherical mirror is reduced, and the coupling element located on it should be closer to the OR axis.

Conclusions

The experimental research covered in this paper makes it possible the following statements.

1. When the coupling element is placed off-center on the curvilinear reflector, axially symmetric oscillations are still excited in the cavity that may even lack circular symmetry. These axially symmetric oscillations have not been discussed in the literature yet [33, 39].

2. A distinctive feature of these axially symmetric oscillations is an area with zero electric-field intensity at the OR center [34]. This feature enables us to use the resonant system with these axially symmetric oscillations for measuring the electrophysical parameters of materials, including liquids. A disk-shaped

sample or a liquid-filled cuvette is placed at the center of the flat mirror of this hemispherical OR.

3. The OR, as examined, allows dynamic quality monitoring of various liquids. In this case, a quartz glass tube is placed along the OR axis. By varying the radius of curvature of the spherical mirror and the coupling element location on the mirror, we regulate the size of the area with zero electric-field intensity in relation to the diameter of the tube. This is particularly important when studying high-loss liquids.

REFERENCES

1. Wang, Y., and Afsar, M.N., 2003. Measurement of Complex Permittivity of Liquids Using Waveguide Techniques. *Progress in Electromagnetics Research (PIER)*, **42**(1), pp. 131—142. DOI: 10.2528/PIER03010602
2. Gennarelli, G., Romeo, S., Scarfi, M.R., and Soldovieri, F., 2013. A Microwave Resonant Sensor for Concentration Measurements of Liquid Solutions. *IEEE Sens. J.*, **13**(5), pp. 1857—1864. DOI: 10.1109/JSEN.2013.2244035
3. Arumugam, J., Edhayaraj, N.R., Shanmugavadivelu, S., and Sathyanarayanan, V., 2023. Design of Microwave Electromagnetic Sensor for Liquid Characterization. *Journal of High-Frequency Communication Technologies*, **1**(3), pp. 73—83. DOI: 10.58399/TLCX9900
4. Volkov, V.V., Suslin, M.A., and Dumbolov, J.U., 2020. Microwave Resonance Method for Measuring Microliter Volumes of Free Moisture of Aviation Fuels. *Meas. Tech*., **63**(7), pp. 226—234. DOI: 10.1007/s11018-020-01775-3
5. Al-Mously, S.I.Y., 2012. A Modified Complex Permittivity Measurement Technique at Microwave Frequency. *Int. J. New Comput. Archit. Appl.* (IJNCAA), **2**(2), pp. 389—401. Available from: https://scispace.com/papers/a-modified-complex-permittivity-measurement-technique-at-2mhob8 glc2
6. Yashchyshyn, Ye., and Godziszewski, K., 2018. A New Method for Dielectric Characterization in Sub-THz Frequency Range. *IEEE Trans. Terahertz Sci. Technol*., **8**(1), pp. 19—26. DOI: 10.1109/TTHZ.2017.2771309
7. Jebbor, N., Bri, S., Mediavilla, A., and Chaib,i M., 2013. A Fast Calibration-Independent Method for Complex Permittivity Determination at Microwave Frequencies. *Measurement*, **46**(7), pp. 2206—2209. DOI: 10.1016/j.measurement.2013.04.009
8. Elmajid, H., Terhzaz, J., and Ammor, H., 2014. Optimization Technique to Estimate the Complex Permittivity of Dielectric Materials at X-Band Using Rectangular Waveguide. *Int. J. Appl. Eng. Res.*, **9**(24), pp. 26709—26718. Available from: http://www.ripublication.com/Volume/ijaerv9n24.htm
9. Benali, L.A., Tribak, A., Terhzaz, J., and Mediavilla, A., 2020. An Accurate Method to Estimate Complex Permittivity of Dielectric Materials at X-band Frequencies. *Int. J. Microw. Opt. Technol.*, **15**(1), pp. 10—16. Available from: https://www.ijmot.com/VOL-15-NO-1.aspx
10. Krupka, J., 2021. Microwave Measurements of Electromagnetic Properties of Materials. *Materials*, **14**(17), pp. 1—21. DOI: 10.3390/ma14175097
11. Breslavets, A.A., Eremenko, Z.E., Rudnev, G.O., Natarov, M.P., Glamazdin, V.V., Shubnyi, O.I., Voitovych, O.A., Gang, Zhu, Rong, Li, and Prokopenko, A.A., 2022. Hemispherical X band Microwave Small Sized Open Resonator for Wide Range from 1 to 20 Permittivity Characterization of Solid-State Dielectrics. *Low Temp. Phys*., **48**(1), pp. 43—50. DOI: 10.1063/10.0008963
12. Alimenti, A., Pittella, E., Torokhtii, K., Pompeo, N., Piuzzi, E., and Silva, E., 2023. Dielectric Loaded Resonator for the Measurement of the Complex Permittivity of Dielectric Substrates. *IEEE Trans. Instrum. Meas.*, **72**(1), pp. 1—9. DOI: 10.1109/TIM.2023.3236301
13. Drobakhin, O.O., 2025. Development of Measurement Methods in Microwave and Terahertz Ranges of Electromagnetic Waves in Ukraine (Review). *Radio Electron. Commun. Syst.*, **67**(4), pp. 161—179. DOI: 10.3103/S0735272724040034
14. Kumar, A., and Sharma, S., 2007. Measurement of Dielectric Constant and Loss Factor of the Dielectric Material at Microwave Frequencies. *Prog. Electromagn. Res.*, **69**, pp. 47—54. DOI: 10.2528/PIER06111204
15. Bendaoued, M., Terhzaz, J., and Mandry, R., 2017. Determining the Complex Permittivity of Building Dielectric Materials using a Propagation Constant Measurement. *Int. J. Electr. Comput. Eng.*, **7**(4), pp. 1681—1685. DOI: 10.11591/ijece.v7i4.pp1681-1685
16. Stumper, U., 1973. A TE_{01n} Cavity Resonator Method to Determine the Complex Permittivity of Low Loss Liquids at Millimeter Wavelengths. *Rev. Sci. Instrum*., **44**(2), pp. 165—169. DOI: 10.1063/1.1686073
17. Abbas, Z., Pollard, R.D., and Kelsall, R.W., 2001. Complex Permittivity Measurements at Ka-Band Using Rectangular Dielectric Waveguide. *IEEE Trans. Instrum. Meas.*, **50**(5), pp. 1334—1342. DOI: 10.1109/19.963207
18. Vuks, M.V., 1984. *Electrical and Optical Properties of Molecules and Condensed Media*. Leningrad, USSR: Leningrad University Publishing House, 1984, pp. 60—62.
19. Afsar, M.N., Button, K.J., 1985. Millimeter Wave Dielectric Measurement of Materials. *Proc. IEEE*, **73**(1), pp. 131—153. DOI: 10.1109/PROC.1985.13114
20. Afsar, M.N., Li, X., and Chi, H., 1990. An Automated 60 GHz Open Resonator System for Precision Dielectric Measurements. *IEEE Trans. Microwave Theory Tech*., **38**(12), pp. 1845—1853. DOI: 10.1109/22.64565

21. Afsar, M.N., Chen, S., and Wang, Y., 2005. An Improved 60 GHz Open Resonator System for Accurate Measurement of Dielectric Permittivity. In: *AP-S Int. Symp.*, Conf. Proc. Washington, DC, USA, 03—08 July 2005, pp. 1—5. DOI: 10.1109/APS.2005.1552842
22. Vlasov, S.N., Parshin, V.V., and Serov, E.A., 2010. Methods for Investigating Thin Dielectric Films in the Millimeter Range. *Tech. Phys*., **55**(12), pp. 1781—1787. DOI: 10.1134/S1063784210120121
23. Yang, B.B., Katz, S.L., Willis, K.J., Weber, M.J., Knezevic, I., and Hagness, S.C., 2012. A High-Q Terahertz Resonator for the Measurement of Electronic Properties of Conductors and Low-Loss Dielectrics. *IEEE Trans. Terahertz Sci. Technol*., **2**(4), pp. 449—459. DOI: 10.1109/TTHZ. 2012.2199578
24. Parshin, V.V., and Serov, E.A., 2012. Resonance Method for Studying Dielectric Liquids in Millimeter and Submillimeter Wave Ranges. *Radiophys. Quantum Electron*., **54**(8–9), pp. 632—637. DOI: 10.1007/s11141-012-9324-x
25. Karpisz, T., Salski, B., Kopyt, P., and Krupka, J., 2019. Measurement of Dielectrics from 20 to 50 GHz with a Fabry–Pérot Open Resonator. *IEEE Trans. Microwave Theory Tech*., **67**(5), pp. 1901—1908. DOI: 10.1109/TMTT.2019.2905549
26. Givot, B.L., Gregory, A.P., Salski, B., Zentis, F., Pettit, N., and Karpisz, N., 2021. A Comparison of Measurements of the Permittivity and Loss Angle of Polymers in the Frequency Range 10 GHz to 90 GHz. In: *15th European Conf. Antennas and Propagation (EuCAP),* Conf. Proc. Dusseldorf, Germany, 22—26 March 2021, pp. 1—5. DOI: 10.23919/EuCAP51087.2021.9411298
27. Kayro, N.S., Teterina, D.D., Badin, A.V., and Bilinskii, K.V., 2021. Automated system based on open resonator for measuring the electrophysical parameters of sheet dielectrics. *J. Phys.: Conf. Ser*., **1989**(1), pp. 012020 (1—5). DOI: 10.1088/1742-6596/1989/1/012020
28. Karpisz, T., Salski, B., Kopyt, P., Krupka, J., and Wojciechowski, M., 2022. Measurement of uniaxially anisotropic dielectrics with a Fabry-Perot open resonator in the 20—50 GHz range. *IEEE Microw. Wirel. Compon. Lett.*, **32**(5), pp. 441—444. DOI: 10.1109/LMWC.2022.3155938
29. Elwood, B.D., Grimes, P.K., Kovac, J., Eiben, M., and Meiners, G., 2024. Fabry–Perot Open Resonant Cavities for Measuring the Dielectric Parameters of mm-Wave Optical Materials. *ArXiv:2411.01058v1 [physics.optics]*, pp. 1—12. DOI: 10.48550/arXiv.2411.01058
30. Chigryai, E.E., Garin, B.M., and Denisyuk, R.N., 2018. Measurement of Dielectric Loss at Millimeter Range in the Low Loss Materials with Arbitrary Ratio of Wavelength and Sample Thickness. *Journal of Radio Electronics (JRE)*, 10, pp. 1—7. DOI: 10.30898/1684-1719.2018.10.10
31. Kuzmichev, I.K., and Popkov, A.Yu., 2018. Resonant Systems for Measurement of Electromagnetic Properties of Substances at V-Band Frequencies. Chapter 3. In: *Emerging Microwave Technologies in Industrial, Agricultural, Medical and Food Processing*. London, United Kingdom: Intech Open Publ., 2018, pp. 27—53. DOI: 10.5772/intechopen.73643
32. Kuzmichov, I.K., Kogut, O.E., Muzychishin, B.I., Popkov, O.Yu., and Senkevych, O.B., 2023. The TE01 wave excitation in a circular waveguide using higher-order modes of an open resonator. *Radio Phys. Radio Astron*., **28**(3), pp. 243—256. DOI: 10.15407/rpra28.03.243
33. Menzel, R., 2007. *Photonics: Linear and Nonlinear Interactions of Laser Light and Matter*. 2nd ed. Berlin, Germany: Springer-Verlag Berlin and Heidelberg GmbH & Co. KG, pp. 395—409. DOI: 10.1007/978-3-540-45158-7
34. Muzychishin, B.I., Kuzmichev, I.K., Senkevych, O.B., and Pogarsky, S.A., 2022. Spectrum of OR Oscillations with a Segment of a Circular Waveguide. In: *2022 IEEE 9th Int. Conf. Problems of Info communications Science and Technology (PIC S&T '2022)*: Conf. Proc. Kyiv, Ukraine, 10—12 Oct. 2022, pp. 524—528. DOI: 10.1109/PICST57299.2022.10238663
35. Valitov, R.A. (ed.), Dyubko, S.F., Kamyshan, V.V., Kuzmichev, V.M., Makarenko, B.I., Sokolov, A.V., and Sheiko, V.P., 1969. *Submillimeter Wave Technique*. Moscow, USSR: Sov. radio Publ., pp. 219—229.
36. Yang, Z., Lin, C., and Zho, Y., 1985. A Method for Measurement of Q-Factor at Millimeter Wavelength. In: *10th Int. Conf. Infrared and Millimeter Waves*, Conf. Proc. Lake Buena Vista, Florida, USA, 9—13 Dec. 1985, pp. 350—351. DOI: 10.1109/IRMM.1985.9126718
37. Kuzmichev, I.K., 2002. The Probe Diameter Choosing for the Investigation of the Field Distribution in the Small Aperture Open resonator. *Telecommunications and Radio Engineering*, **58**(7—8), pp. 59—63. DOI: 10.1615/TelecomRadEng.v58.i7-8.50
38. Tarasov, L.V., 1981. *Physics of processes in coherent optical radiation generators*. Moscow, USSR: Radio i Svyaz' Publ., 1981, pp. 141—212.
39. Weber, H., Herziger, G., Poprawe, R. (eds.), 2006. *Laser Physics and Applications. Laser Fundamentals.* Part 2. Group VIII, Vol. 1. Berlin, Germany: Springer-Verlag, Berlin, Heidelberg, New York, pp. 149–161 ISSN 1619-4802.
40. Kogelnik, H., 1964. Coupling and conversion coefficients for optical modes. In: *Quasi-Optics*, Proc. Symp. New York, NY, 8—10 June 1964. Microwave Research Institute Symposia Series. Vol. 14. Brooklyn, NY: Polytechnic Institute of Brooklyn, Polytechnic Press, pp. 333–347. ISBN 10 0470274298.

Received 14.09.2025

І.К. Кузьмичов[1], *О.С. Лукаш*[1], *О.Б. Сенкевич*[1],
О.А. Войтович[1], *Т.М. Наритник*[2], *Г.І. Чурюмов*[3]
[1] Інститут радіофізики та електроніки ім. О.Я. Усикова НАН України
вул. Акад. Проскури, 12, м. Харків, 61085, Україна
[2] Навчально-науковий інститут телекомунікаційних систем НТУУ
«Київський політехнічний інститут імені Ігоря Сікорського»
просп. Берестейський, 37, м. Київ, 03056, Україна
[3] Харбінський технологічний інститут
вул. Ксіда, 92, Нанган, м. Харбін, Хейлунцзян, 150001, Китай

АКСІАЛЬНО-СИМЕТРИЧНІ КОЛИВАННЯ У ВІДКРИТОМУ РЕЗОНАТОРІ

Предмет і мета роботи. Предметом досліджень є поведінка аксіально-симетричних коливань у напівсферичному відкритому резонаторі (ВР), що інтегрований до хвилевідної лінії передачі і працює в наскрізному режимі. Апертури дзеркал ВР дорівнюють 60 мм, радіус кривизни сферичного відбивача становить 85 мм. Два щілинних елементи зв'язку розміром 3.6×0.17 мм розташовані симетрично на відстані 13.2 мм від осі ВР. Метою роботи є дослідження аксіально-симетричних коливань, які збуджуються у такому напівсферичному ВР щілинними елементами зв'язку. Актуальність цих досліджень пов'язана з вимірюванням методом ВР параметрів діелектриків у ВВЧ-діапазоні.

Методи та методологія. Для вирішення поставлених у роботі завдань використано основні методи квазіоптики. Для вимірювання структур електричних полів розглянутих типів коливань застосовано метод пробного тіла. Резонансні коефіцієнти передачі відкритих коливальних систем і фізичні явища, що в них відбуваються, досліджуються за допомогою стандартних методів НВЧ-вимірювань.

Результати. Дослідження проводили на частоті 70.622 ГГц. Для вимірювання амплітудного розподілу збуджуваних у розглянутому резонаторі коливань використовували пробне тіло діаметром 1 мм. У резонаторі збуджувалися коливання з великими поперечними індексами. Показано, що при неосьовому збудженні у ВР існують аксіально-симетричні коливання. Експериментально встановлено відмінну особливість таких коливань: у центрі резонатора існує область з нульовою інтенсивністю електричного поля. Для досліджуваного коливання $TEM^*_{0,1,12}$ ця область має діаметр 6 мм.

Висновки. Відкритий резонатор з аксіально-симетричними коливаннями є ефективним для вимірювання електрофізичних параметрів матеріалів, включаючи рідини. Установлено, що розміщення дископодібного зразка або кювети, заповненої рідиною, в центрі плоского дзеркала напівсферичного ВР не тільки не порушує робоче коливання, але й до того ж сприяє додатковій селекції спектра коливань ВР. Розглянутий ВР також може бути використаний для динамічного контролю якості різних рідин. У цьому випадку вздовж осі резонатора розташовують тримач у вигляді кварцової скляної трубки.

Ключові слова: *міліметровий діапазон, відкритий резонатор, типи коливань, елемент зв'язку, коефіцієнт передачі, пробне тіло.*